Jerzy BARGLIK

Silesian University of Technology, Department of Industrial Informatics

doi:10.15199/48.2018.04.13

Induction hardening of steel elements with complex shapes

Abstract. *As an example of induction hardening of steel elements with complex shapes the induction contour hardening of gear wheels was selected. The model of the process was proposed and simulation results elaborated by means of professional computer software for coupled physical fields were presented. Quite reasonable accordance between computations and measurements was obtained.*

Streszczenie. *Jako przykład hartowania indukcyjnego elementów stalowych o złożonych kształtach wybrano proces hartowania konturowego kół zębatych. Zaproponowano model procesu oraz przedstawiono wyniki symulacji z wykorzystaniem programów do obliczania sprzężonych pól fizycznych. Uzyskano zadowalającą zbieżność wyników pomiarów i obliczeń. (**Hartowanie indukcyjne elementów stalowych o złożonych kształtach**).*

Keywords: induction contour hardening, induction heating, electromagnetic field, austenitization
Słowa kluczowe: hartowanie indukcyjne konturowe, nagrzewanie indukcyjne, pole elektromagnetyczne, austenityzacja.

Introduction

Induction hardening is a such kind of electromagnetic materials processing (EPM) which is characterized by induction heating of the steel elements and then immediate cooling. Induction surface hardening means treating of thin surface zone of the element only keeping soft and unchanged the microstructure in internal zones. It is modern heat treatment technology especially often applied for axi-symmetric and flat workpieces, however recently often used also for steel elements of complex shapes [1]. The advantage of the induction hardening technology is a location of the heat source very close to the hardening zone, directly opposite to the inductor. Thickness of the hardened zone depends on many factors including four of them which are more important::
- frequency of supplied current,
- power delivered to the treated element,
- total time of heating,
-.material properties and heat transfer parameters.

Such the technology makes possible to generate extremely high power density in the thin hardened zone due to application of modern high frequency transistor sources and short heating times. As a result hardened zones having very small thickness could be obtained [2].

Selection of the process properties

Induction hardening of steel elements also with complex shapes like gear wheels seems to be nowadays more often applied form of surface hardening. Exemplary temperature dependence on time in the thin surface zone of the body for induction hardening by single frequency treatment is presented in Fig. 1.

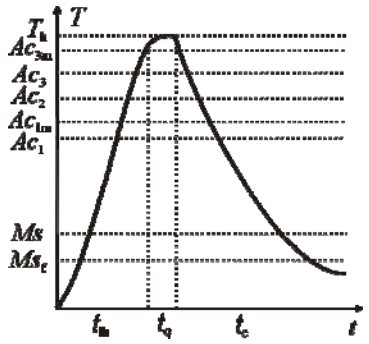

Fig..1. Temperature dependence on time in the surface zone during single frequency induction hardening (notations in the text).

The time of induction heating t_{ih} is typically short (a couple of seconds) or very short (hundreds of milliseconds). For instance if we supply the induction hardening system from the transistor source with power of about several hundreds kW, the time of induction heating could be reduced to the level of hundreds milliseconds [2] During such a short time the surface zone of the material is heated up to hardening temperature T_h being bigger or at least equal to the modified upper critical temperature Ac_{3m} making possible to complete the austenite transformation in the condition of rapid induction heating and very short austenitization time t_q

$$T_h = T\big|_{t=t_{ih}+t_q} \geq Ac_{3m} \tag{1}$$

Condition (1) is satisfied at the surface of the body and in thin surface zone. At the same time ($t = t_{ih} + t_q$) for deeper zones of the material the temperature reaches lower values

$$Ac_{3m} \geq T\big|_{t=t_{ih}+t_q} \geq Ac_{1m} \tag{2}$$

where: Ac_{1m} – modified lower criterial temperature

Austenite transformation begins, but prior microstructure changes only partly. It contains not only the austenite, but also pearlite and ferrite. For deeper layers of the material temperature does not reach even the modified lower criterial temperature Ac_{1m}. The austenite transformation does not begin

$$T\big|_{t=t_{ih}+t_q} \leq Ac_{1m} \tag{3}$$

The microstructure of the material does not change at all.

Values of criterial temperatures characterized beginning (Ac_1) and completion (Ac_3) of austenite transformation for conventional process are depicted in Fig.1. They are lower than their modified values Ac_{1m} and Ac_{3m} respectively. Dependence of the criterial temperatures on heating rate determined from the Time-Temperature-Austenitization (TTA) diagram for steel 41Cr4 is presented in Fig.2

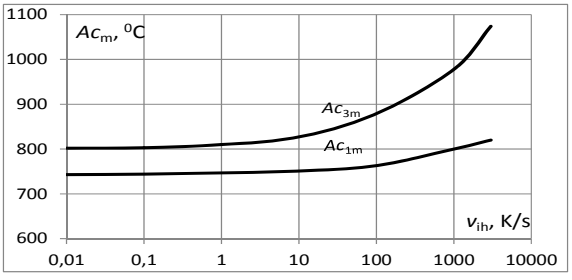

Fig.2. Dependence of the modified criterial temperatures Ac_{1m} and Ac_{3m} on heating rate.

For the low heating rate v_{ih} = 1 K/s the modified upper criterial temperature Ac_{3m} = 803^{0}C and it is almost the same as for the conventional heating in furnaces. If the heating rate is distinctly bigger (v_{ih} = 1000 K/s) the modified upper critical temperature Ac_{3m} is 173 K higher than Ac_3. In the same conditions as previously the modified lower criterial temperature Ac_{1m1} = 740^{0}C and Ac_{1m2} = 800^{0}C and it is 54 K higher than A_{c1}. For the hardening process important influence has also two other parameters. The first of them is the prior microstructure. At Ac_2 temperature (see Fig.1) the magnetic transformation begins influencing on uniformity of austenite microstructure [3]. The second one is a way of cooling. Temperatures of beginning and terminating of the martensite transformation (*Ms* and Ms_f respectively) are depicted in Fig.1. For the cooling rate v_c = 297 K/s *Ms* = 381^{0}C, and Ms_f = 120^{0}C. Dependence of hardness on cooling rate determined from the Cooling Time Temperature continuous (CTTc) diagram is presented in Fig.3. .

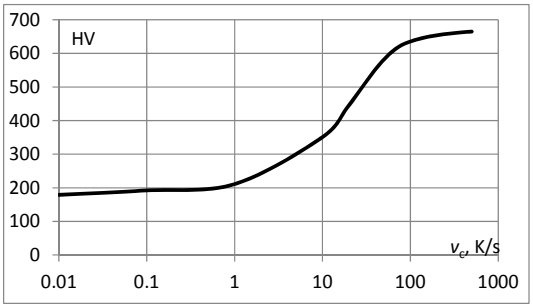

Fig. 3. Dependence of hardness on cooling rate for steel 41Cr4..

The uniform martensitic microstructure at the surface zone is obtained if the cooling rate is big enough and the final temperature T_f is the zone is smaller than Ms_f.

(4) $$v_c \geq v_{cmin} \quad T_f < Ms_f$$

For steel 41Cr4 v_{cmin} = 70 K/s

Mathematical model

As an example of the induction hardening process contour spin induction hardening of small gear wheels made of steel 41Cr4 is selected. Algorithm of the calculation model is shown in Fig.4. Computations begin with a completion of input data. Prior microstructure of the material is taken into account [3]. Material properties and their temperature dependences are measured or taken from specialized databases [4]. Based upon electromagnetic field computations the volumetric density of power density p_V released in the treated body is determined. In general it consists of two components connected with hysteresis p_H and induction p_J phenomena. For the analyzed case the hysteresis component of the volumetric power density is distinctly lower than the induction one and it could be neglected.

(5) $$p_V = p_h(|\boldsymbol{H}|, f) + p_i(|\boldsymbol{J}_{ind}|, \gamma) = \mu f |\boldsymbol{H}|^2 + \frac{|\boldsymbol{J}_{ind}|^2}{\gamma} \approx \frac{|\boldsymbol{J}_{ind}|^2}{\gamma}$$

where $|\boldsymbol{H}|$, $|\boldsymbol{J}_{ind}|$ modules of the magnetic strength and induced current density respectively, *f* – field current frequency, γ – electric conductivity.

Non-linear dependence of the magnetic permeability on the magnetic strength and temperature was taken into account, but its dependence on frequency was neglected.

(6) $$\mu = \mu(|\boldsymbol{H}|, T, f) \approx \mu(|\boldsymbol{H}|, T)$$

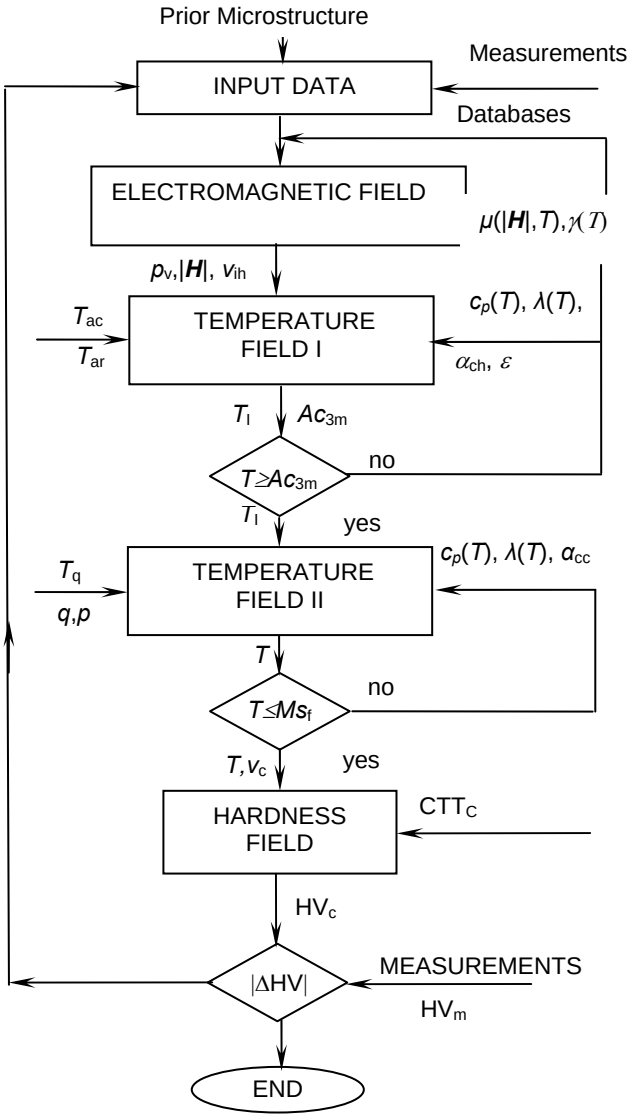

Fig. 4. Algorithm of the computation model.

Non-linear dependences of material properties of steel 41Cr4 (the electric conductivity, the thermal conductivity, the density, the specific heat and the relative magnetic permeability) on temperature were also taken into account. They were measured for the samples taken from the same part of the material which was used for production of gear wheels (see Figs. 5 – 9 respectively)

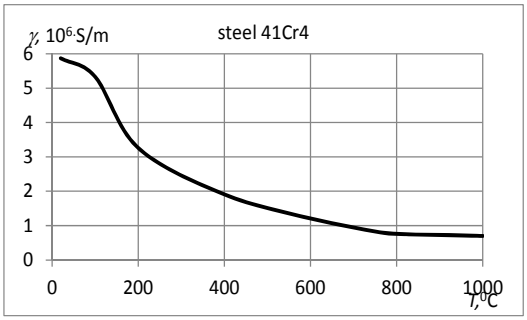

Fig.5. Dependence of electric conductivity on temperature.

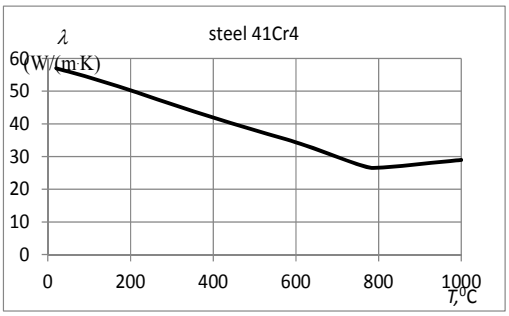

Fig.6. Dependence of thermal conductivity on temperature.

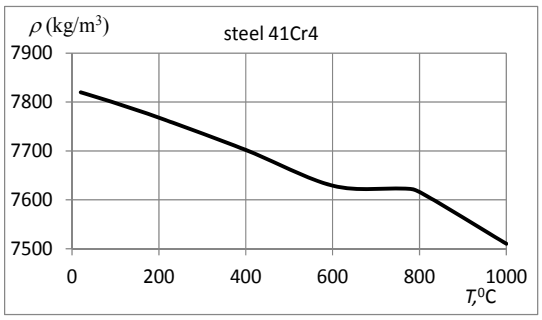

Fig.7. Dependence of density on temperature.

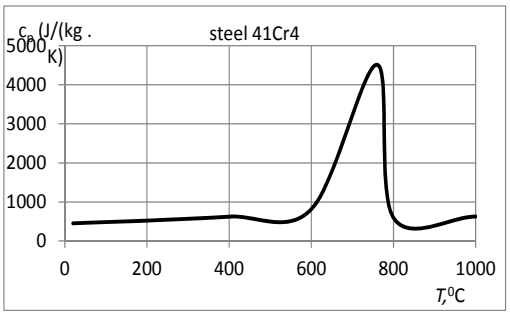

Fig.8. Dependence of specific heat on temperature

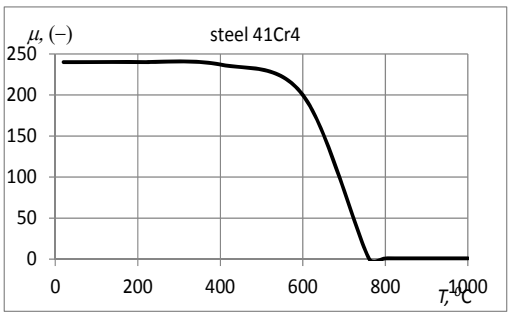

Fig.9. Dependence of relative magnetic permeability on temperature for $|\boldsymbol{H}|$ = const.

Heat transfer between the body and surroundings was analyzed by the 3rd kind boundary condition in the form:

$$-\lambda \cdot \frac{\partial T}{\partial n} = \alpha_{\mathrm{ch}} \left(T - T_{\mathrm{ac}}\right) + \sigma_{\mathrm{o}} \varepsilon \left(T^4 - T_{\mathrm{ar}}^4\right) \tag{6}$$

where: n denotes outward normal to the boundary, α_{ch} – convection heat transfer coefficient (heating), σ_{o} – Stefan-Boltzmann constant, ε – emissivity, $T_{\mathrm{ac}}, T_{\mathrm{ar}}$ – temperature of convection and radiation environment respectively

Computations of coupled electromagnetic and temperature field for induction heating terminate when the condition (1) is satisfied in the whole hardened zone. The next step is calculation of temperature field for cooling. For that part of computations radiation was neglected. Heat transfer between the body and the quenchant α_{cc} is described by:

$$-\lambda \cdot \frac{\partial T}{\partial n} = \alpha_{\mathrm{cc}}(p, q) \cdot \left(T - T_{\mathrm{q}}\right) \tag{7}$$

where: T_{q}, p, q - temperature, pressure and flow-rate of quenchant respectively.

Exemplary dependence on the convection heat transfer for cooling by spraying on temperature is presented in Fig. 10.

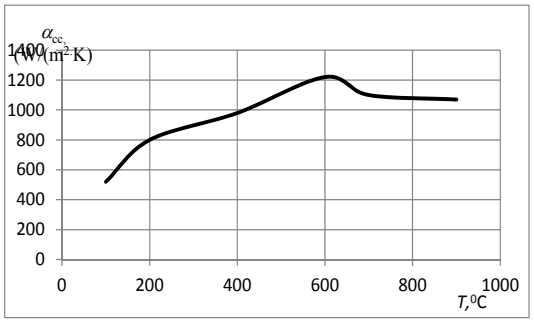

Fig. 10. Exemplary dependence of the convection heat transfer coefficient during cooling on temperature.

For the analyzed case - induction hardening of gear wheels different average values of convection heat transfer coefficient for each surface of the tooth is considered. Its dependence on temperature is neglected. Computations of temperature field are terminated when the average temperature in hardened zone satisfies the condition (4). Hardness distribution in the hardened zone is determined by means of curve shown in Fig.3 obtained from the measured CCT_c diagram.

Illustrative example

Let us consider the illustrative example of the consecutive dual frequency induction heating (CDFIH) of small gear wheel made of steel 41Cr4 with 0.4 % of carbon content. First the gear wheel is heated by the medium frequency ring (MF) inductor up to the temperature not higher than the modified lower criterial temperature Ac_{1m}, and then with a very short austenitization (about 0.1 s) is heated by the high frequency ring (HF) inductor up to the hardening temperature T_{h}.. Numerical simulation and its experimental validation were provided for following parameters and dimensions of the hardening system:

gear wheel: teeth number – 16, module – 2 mm, external diameter – 0.0356 m, width of tooth ring – 0.006 m,

MF inductor: height 0.007 m, internal diameter 0.0395 m, external diameter 0.054 m,

HF inductor: height – 0.021 m, internal diameter – 0.0395 m, external diameter – 0.061 m, concentrator – Fluxtrol 50.

selected parameters: MF heating: power – 28 kW, current – 1385 A, frequency – 36 kHz, time – 4.1 s, final temperature – 520^{0}C, modified lower criterial temperature – 754^{0}C, HF heating: power – 19700 kW, current – 500 A, frequency – 280 kHz, time – 0.7 s, modified upper criterial temperature – 925^{0}C, hardening temperature – 960^{0}C, break between MF and HF heating – 0.1 s, break between heating and cooling – 0.1 s, total time – 5 s, tempering: temperature – 160^{0}C, time – 7200 s.
Temperature distribution within the volume of tooth at the moment when cooling starts is shown in Fig. 11

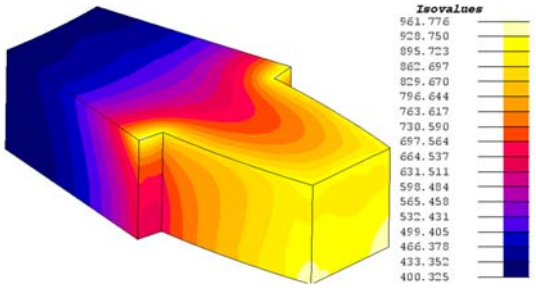

Fig. 11. Temperature distribution within the tooth for total time of heating $t = t_{MF}+t_{b1}+ t_{HF}+t_{b2} = 5$ s.

The temperature distribution along the working surface of the tooth is non-uniform (Fig. 12).

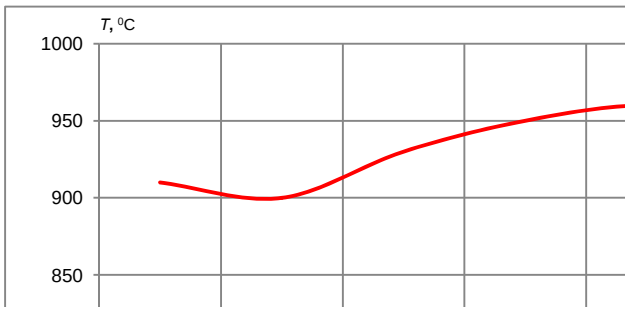

Fig. 12. Temperature distribution along the working surface for total time t -= 5 s, A on cut , B…E on working surface, F –- on top. .

The highest temperature in point E located near the top of the tooth was noticed. The lowest temperature was in the edge of the tooth between points A and B and it was lower than the modified upper criterial temperature. The temperature distribution in direction inside the tooth taken from the point F located at the top is shown in Fig. 13.

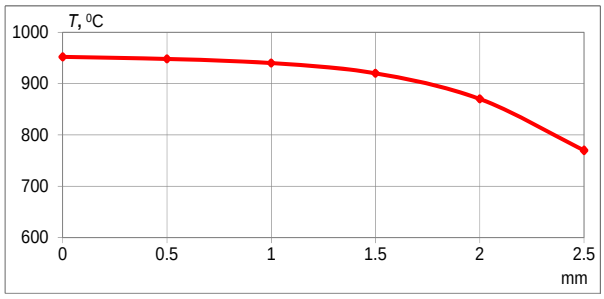

Fig. 13. Temperature distribution in direction inside the tooth for point F located at the top of the tooth (total time $t = 5$ s).

The polymer solution Aqua Quench 140 was applied for spraying. Its temperature –- 30^{0}C, concentration –- 12 %, convection heat transfer coefficient –- 1200 W/(m^2·K).
The calculated hardness distribution along the line A – F is shown in Fig. 14.

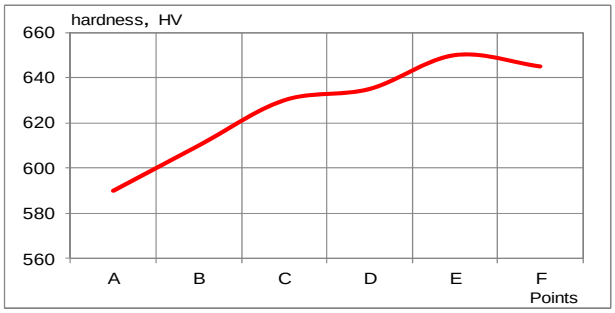

Fig. 14 Calculated hardness distribution along the working surface of the tooth.

The gear wheels were hardened only (IH) or immediately after hardening were tempered (IH +T). Comparison of the results were presented in Tab. I and in Fig. 15.

Table I Calculated and measured hardness distribution

Points	A cut	B	C	D	E	F top
HV comp	590	610	630	635	650	645
HV (IH only)	560	590	610	630	635	635
HV (IH + T)	530	540	580	600	610	612

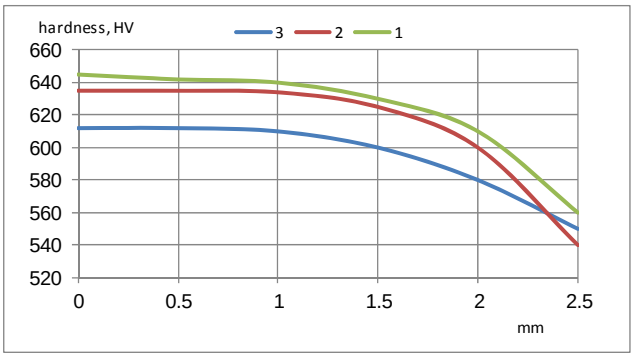

Fig. 15 Calculated and measured hardness distribution in depth of the tooth 1 – computations, 2 – IH, 3 – IH + T).

Summary

As the example of induction hardening of steel elements with complex shapes the induction contour hardening of gear wheels was selected. The model of the process was proposed and described. Simulation results elaborated by software for coupled physical fields were presented. Quite reasonable accordance between computations and experiments was obtained. Next research will be aimed on accuracy improvement of the numerical modeling.

Acknowledgment

The paper was granted by the project PBS2/A5/41/2014 supported by the National Center of Research and Development in Warszawa, Poland.

***Author**: professor Jerzy Barglik, Silesian University of Technology, Department of Industrial Informatics, 8 Krasińskiego street, 40-019 Katowice, E-mail: jerzy.barglik@polsl.pl*

REFERENCES

[1] Barglik J.: Mathematical modelling of induction surface hardening, *COMPEL-The international journal for computation and mathematics in electrical and electronic engineering*, 35, (2016), No. 4, 1403 – 1417

[2] Rudnev V., Totten G.: *Induction Heating and Heat Treatment*. ASM International, Vol. 4C, (2014)

[3] Rudnev V.: Be aware of the 'fine print' in the science of metallurgy in induction hardening part I, *Industrial Heating*, 72, (2005), No.3, 37 – 42